Astron. Nachr. / AN **328**, No. 3/4, 319 – 322 (2007) / **DOI** 10.1002/asna.200610737

# The solar acoustic simulator: applications and results

**S.M. Hanasoge**[1,2,⋆] and **T.L. Duvall, Jr.**[3]

[1] W.W. Hansen Experimental Research Laboratory, Stanford University, CA 94305, USA
[2] Department of Mechanical Engineering, Stanford University, CA 94305, USA
[3] Solar Physics Laboratory, NASA/Goddard Space Flight Center, Greenbelt, MD 20771, USA

Received 2006 Oct 17, accepted 2007 Jan 2
Published online 2007 Feb 28

**Key words** Sun: oscillations – Sun: helioseismology – Sun: interior

It is important to understand the limits and accuracy of helioseismic techniques in their ability to probe the solar interior. The availability of a method that is able to compute the solar acoustic wave field in the presence of thermal or flow perturbations affords us a means to place bounds on detectability and accuracy of inferences of interior perturbations. We describe the technique used to simulate wave propagation within a spherical shell that extends from a desired depth (not including the center) into the solar atmosphere and which possesses a solar like stratification.



## 1 Introduction

With the advent of time-distance helioseismology (Duvall et al. 1993), it has become possible to infer the subtle structure and dynamics of the solar interior. However, while significant effort has been channelled into performing inversions to recover these interior properties, little has been done in the direction of verifying the accuracy of these inferences or systematically utilising the forward approach to understand the interactions of waves with various perturbations.

It is important that the forward model be designed to mimic the Sun as closely as possible because data produced from such a model will likely easily lend themselves to interpretation in the context of the solar case. On the other hand, it is equally useful to leave the system simple enough that we are able to understand the individual contributions of various perturbations on helioseismic metrics such as travel times, mode frequencies etc.

The utility of the forward approach cannot be understated, for it paves the way for us to gauge the ability of helio- and astero-seismology to infer the interior properties of the Sun and other stars. In relation to the Sun, we are already investigating the signal to noise properties of deep active regions, holographic far-side signatures of active regions (sunspots and the like), detection of convection and line-of-sight projection anomalies.

## 2 Description of the code

### 2.1 Equations

To model the behaviour of the acoustic wavefield, we solve the 3D unsteady linearized Euler equations in spherical geometry to obtain a spatio-temporal description of the surface wave-field. Equations (1), (2), and (3) are the equations of continuity, momentum and energy respectively,

$$\frac{\partial \rho}{\partial t} = -\boldsymbol{\nabla}\cdot(\rho_0 \boldsymbol{v}) - \boldsymbol{\nabla}\cdot(\rho \boldsymbol{v}_0), \tag{1}$$

$$\begin{aligned}\frac{\partial \boldsymbol{v}}{\partial t} = &- \boldsymbol{\nabla}(\boldsymbol{v}_0\cdot\boldsymbol{v}) - \boldsymbol{\omega}_0\times\boldsymbol{v} - \boldsymbol{v}_0\times\boldsymbol{\omega} \\ &- \frac{\rho}{\rho_0}\left(\boldsymbol{\nabla}(\frac{1}{2}v_0^2) + \boldsymbol{\omega}_0\times\boldsymbol{v}_0\right) \\ &- \frac{1}{\rho_0}\boldsymbol{\nabla}p - \frac{\rho}{\rho_0}g\hat{\boldsymbol{r}} - \Gamma(r)\boldsymbol{v} + S(r,\theta,\phi,t)\hat{\boldsymbol{r}},\end{aligned} \tag{2}$$

$$\frac{\partial p}{\partial t} = -\boldsymbol{v}_0\cdot\boldsymbol{\nabla}p - \boldsymbol{v}\cdot\boldsymbol{\nabla}p_0 - \Gamma_1 p_0 \boldsymbol{\nabla}\cdot\boldsymbol{v} - \Gamma_1 p \boldsymbol{\nabla}\cdot\boldsymbol{v}_0, \tag{3}$$

$$\Gamma_1 = \left(\frac{\partial \ln p}{\partial \ln \rho}\right)_{\mathrm{ad}}. \tag{4}$$

The nomenclature is as follows: $\rho$ is the density, $p$ the pressure, $\boldsymbol{\omega}$ the vorticity, $\Gamma_1 = \Gamma_1(r)$ is the first adiabatic exponent, $g$ is gravity, and $\boldsymbol{v}$ is the vector velocity. All variables with a zero subscript are time-stationary background counterparts of corresponding fluctuating quantities (terms without a subscript). The derivative on the right-hand side of Eq. (4) is evaluated along an adiabatic process curve (as denoted by the subscript 'ad'). The function $\Gamma(r)$ represents absorbent sponges that are placed on either radial end of the computational domain. $S(r,\theta,\phi,t)$ is the wave excitation function, a description of which follows.

### 2.2 Sources

Granulation is thought to be the dominant source of acoustic wave generation with most of the wave excitation occurring in an extremely narrow spherical shell (200 km

⋆ Corresponding author: shravan@stanford.edu

thick) bounded by the surface, and we choose therefore, $S(r,\theta,\phi,t) = \tilde{S}(\theta,\phi,t)f(r)$, where $f(r)$ is a Gaussian with a full width at half maximum of 100 km centered around $r = 0.9997\ \mathrm{R}_\odot$.

As for determining the horizontal component of the excitation function ($S(\theta,\phi,t)$), we note first that granules possess length scales of approximately 1000 km, much smaller than the wavelengths of the acoustic waves we capture with this calculation. Consequently, granules can be modeled as uncorrelated spatial delta functions, resulting in a uniform stochastic excitation in spherical-harmonic space. Keeping this in mind, we compute uncorrelated, frequency band-limited time series for each spherical harmonic coefficient, ensuring that the excitation level in spherical harmonic space is isotropic. In the frequency domain, it is observed that the solar acoustic power spectrum possesses maximum power in the range 2000–5500 $\mu$Hz with a peak in power around 3200$\mu$Hz. In order to mimic this excitation behavior, we generate a Gaussian power spectrum with a mean of 3200 $\mu$Hz and a standard deviation of 1000 $\mu$Hz in frequency space, which we then Fourier transform to produce a time series with the appropriate source spectrum. Figure 1 compares time-distance correlations for MDI medium-$l$ data with simulation data. It can be seen that correlations for a given time and distance are approximately the same in both cases. We do not make direct comparisons between the two datasets because we use an altered model of the Sun in simulations. It is interesting to note that the values of the correlation coefficients are comparable. This indicates that the source excitation model we apply is representative of the solar acoustic excitation mechanism in this range of wave-numbers.

### 2.3 Numerical algorithm

Spherical harmonics form a rotation group and provide equi-areal representation of the spherical surface, eliminating numerical problems associated with the poles. Using this spectral description, horizontal derivatives of various quantities are calculated in spherical harmonic space by applying appropriate recursion relations. Radial derivatives are obtained using sixth order accurate compact finite differences (Lele 1992). Variables are advanced in time through the repeated application of a multi-stage optimized version of the explicit fourth order Runge-Kutta scheme (Berland et al. 2006).

As for the grid, we use Gaussian collocation points in latitude and equally spaced points in longitude. The radial gridpoint distribution is based on the nature of the underlying stratification; the interior grid-spacing is chosen so that the acoustic travel-time between adjacent gridpoints is constant while the near-surface grid spacing is such that the variation in the logarithm of density between adjacent gridpoints is constant. The grid is made to undergo a smooth transition between these two regions via the application of third order splines.

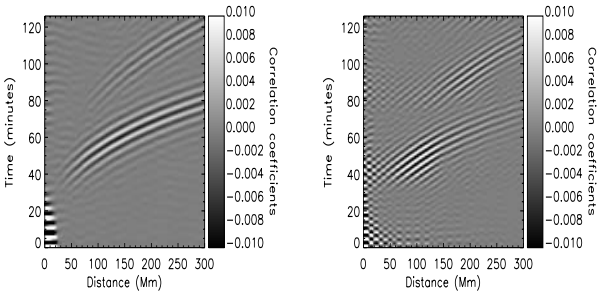


**Fig. 1** Displayed are correlations obtained from MDI Medium-$l$ data on the left panel and simulation data on the right panel. The x-axis is distance in Mm, the y-axis time in minutes and the scale corresponds to the correlation coefficient.

The calculation is computationally intensive requiring the use of parallel architectures. The code has been written according to two parallel standards, OpenMP and Message Passing Interface (MPI). The MPI version of the computation is significantly faster over $341 > l_{\max} > 127$, where $l_{\max}$ is the maximum spherical harmonic degree used in the simulation. We have performed most of our computation on the supercomputer Columbia, located at NASA Ames and locally, on machines located at the Solar group at Stanford University. A more detailed description of the parallel implementation algorithm and numerical methods utilised in the calculation may be found in Hanasoge et al. (2006) and Hanasoge & Duvall (2006).

### 2.4 Background models

The solar stratification in our simulations, described in Hanasoge et al. (2006), is given by an altered form of model S of Christensen-Dalsgaard et al. (1996). The altered stratification is for the most part like model S; it possesses solar like acoustic cutoff frequencies, thermodynamic properties and is hydrostatically balanced. However, in contrast to realistic solar models, it is convectively stable in the near-surface layers. This reconfiguration of the stratification is essential because the time scales of linear convective growth in the near-surface layers coincide with the acoustic timescales of interest and not only corrupt the acoustic signal but renders the calculation highly unstable.

We use time stationary descriptions of both the solar stratification and the perturbations in question (such as sunspots, flows, large scale thermal asphericities in the interior) in the computation. For a more detailed description of the methods used in this simulation and the means of validation, please refer to Hanasoge et al. (2006) and references therein.

## 3 Spectral blocking and radial de-aliasing

Spectral blocking is an aliasing phenomenon that commonly occurs in non-linear calculations, wherein the lack of

 

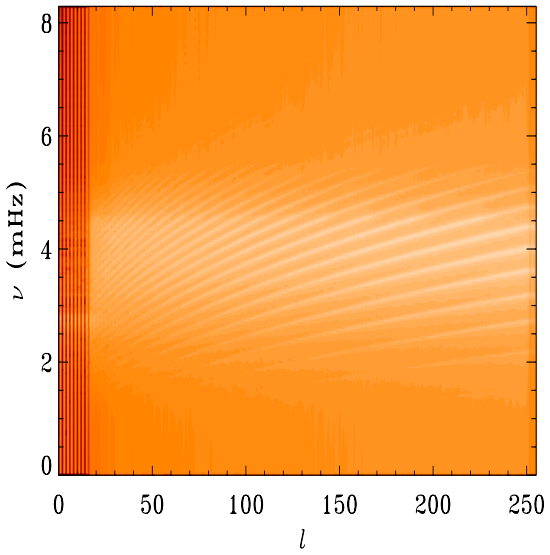


**Fig. 2** Logarithmic power spectrum from for a model that extends from 0.26–1.0033 $R_\odot$. The excitation spectrum is a band that approximately encompasses 2000–5500 $\mu$Hz in frequency and 20–255 in the spherical harmonic degree, $l$. Modes with inner turning points deeper than the lower simulation boundary are absent from this spectrum. Note that because the short time-scale convective instabilities have been removed we see no power at frequencies below 2000 $\mu$Hz. This spectrum was extracted from a 8-hour-long simulation.

resolution results in a super-linear accumulation of energy near the Nyquist frequency. It poses a serious numerical challenge, since the energy growth is very rapid, leaving the computation unstable and inaccurate. We discuss its appearance in our *linear* calculations and how we deal with this issue. Standard Fourier transforms are defined on grids where the travel-time for waves between adjacent grid points is a constant over the grid. In the solar case, the sound-speed is a strong function of radius and consequently, it makes little sense to speak of a Fourier transform on a uniformly spaced radial grid. The Fourier transform in this situation is only made meaningful on a grid stretched such that the travel-time between adjacent grid-points is constant over the grid. The rest of the discussion in this section follows as a consequence of this grid stretching and the consequent interpretation of the Fourier transform on this grid.

As described above, the source function is highly limited in the radial direction resulting in the excitation of waves with a wide spectrum of radial orders. The resolution in the radial direction is restricted by the finiteness of computational resources at our disposal and the scientific interest in investigating these high radial orders. For the applications that we are interested in, both these criteria indicate that these high radial orders are best done away with. Associated with the inability of the radial grid to capture modes containing rapid variations is the phenomenon of aliasing which causes waves beyond the resolvable limit of the grid to fold back across the Nyquist onto the resolvable waves near the Nyquist. This by itself is not a serious problem since we are only interested in a small number of ridges that are situated well away from the radial Nyquist. Typically, aliasing in linear problems is relatively harmless and usually only results in a slight increase in power near the Nyquist.

Interestingly however, in our calculations, Fourier transforms in the radial direction display spectral blocking (shown in Fig. 3), an effect that occurs in numerical solutions of non-linear equations, commonly seen in simulations of turbulence and other non-linear phenomena. It is seen in our computations because of the highly non-constant terms (in the solar case) of the Euler equations, density, pressure and sound speed, that pre-multiply the linear fluctuation terms, like the first term on the right-hand-side of Eq. (1). These non-constant terms act as conveyor belts across the radial spectrum, transferring energy between disparate wavenumbers, and eventually cause this aphysical energy build-up at the Nyquist. The energy accumulation occurs at a non-linear rate, rapidly posing a threat to the accuracy and stability of the calculation.

In order to de-alias the variables, we apply the 11 point de-aliasing filter (Vichnevetsky & Bowles 1982) given by

$$\begin{aligned}\hat{u}_n &= a_0 u_n + \frac{a_1}{2}(u_{n-1}+u_{n+1}) + \frac{a_1}{2}(u_{n-2}+u_{n+2}) \\ &+ \frac{a_2}{2}(u_{n-2}+u_{n+2}) + \frac{a_3}{2}(u_{n-3}+u_{n+3}) \\ &+ \frac{a_4}{2}(u_{n-4}+u_{n+4}) + \frac{a_5}{2}(u_{n-5}+u_{n+5})\,, \end{aligned} \tag{5}$$

with

$$\begin{aligned} a_0 &= 0.753906,\ a_1 = 0.410155,\ a_2 = -0.234375\,, \\ a_3 &= 0.087890,\ a_4 = -0.019531,\ a_5 = 0.001953\,, \end{aligned}$$

where $\hat{u}_n$ and $u_n$ are the filtered and unfiltered variables at grid point $n$, every few time-steps so that any growth near the Nyquist is suppressed. Because of the high order of the filter, the portion of radial spectrum of interest is left largely unaffected. Note that because of the varying sound-speed, we can only apply the filter on the stretched grid over which the acoustic travel-time between adjacent grid points is constant.

## 4 Line asymmetry

Power spectra of the Sun are obtained either through measurements of fluctuations in velocity or in intensity. Mode shapes and line asymmetries in the $l$-$\nu$ power spectrum are a strong function of source depth (e.g. Rast & Bogdan 1998), with velocity and intensity lines displaying phase differences in the asymmetries. By choosing to place sources very close to the surface, we obtain velocity line asymmetries similar to those seen in the Sun, higher on the low frequency side of the mode. By assuming a direct correlation between temperature and intensity fluctuations, Rast & Bogdan (1998) have demonstrated that purely adiabatic oscillations (as in our simulations) result in identical intensity and velocity line asymmetries. An artefact of the simplicity of our adiabatic model and in direct contrast to the Sun,

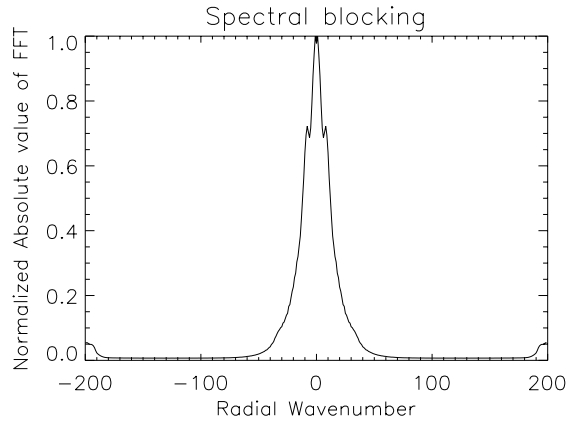


**Fig. 3** Spectral blocking in a linear simulation. This is a classic malaise affecting non-linear calculations, resulting in aphysical energy accumulation near and at the Nyquist.

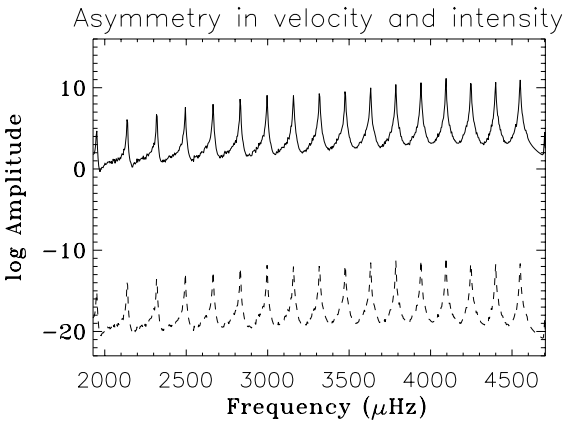


**Fig. 4** Line asymmetry for wave modes with spherical harmonic degree $l = 30$. The mode amplitude is expressed in arbitrary units. The solid line shows modes captured in the velocity spectrum and the dashed line shows modes in intensity (essentially temperature fluctuations). These lines are asymmetric at low frequencies ($< 4000$ $\mu$Hz) and become more symmetric as frequency increases ($/ \sim 4200$ $\mu$Hz).

we also observe no phase difference between velocity and intensity asymmetries (Fig. 4).

## 5 Farside seismology

We are involved in supplementing efforts towards the calibration of farside sunspot detection methods. We place a sunspot, modeled as a local near-surface thermal disturbance, on one hemi-sphere (representing the farside) and analyze the wave-field on the other hemi-sphere (representing the near-side). The thermal disturbance extends 15 Mm into the solar interior and is approximately $8^\circ$ wide. As seen in Fig. 5, the presence of this disturbance creates anisotropies in the time averaged root mean square (RMS) velocities observed at the photosphere. This property may prove to be

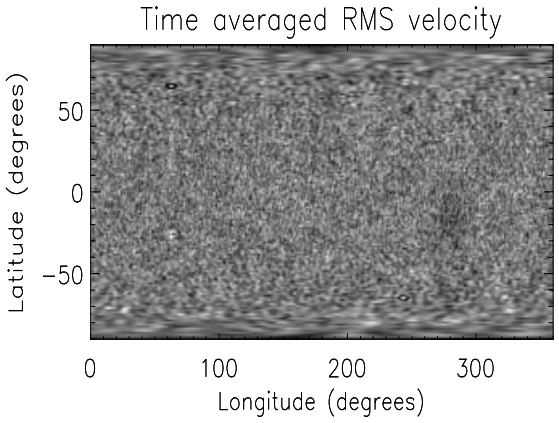


**Fig. 5** Local decrease in the time averaged RMS velocity due to a near surface sound speed increase, located at a latitude of $-15^\circ$ and longitude of $280^\circ$.

useful in the detection of emerging active regions, which are thought to create wave-speed anisotropies.

## 6 Summary and conclusions

We have designed a means to perform *differential* studies of the effects of flows and asphericities on the acoustic wavefield in full spherical geometry. From a practical standpoint, this technique is useful in understanding signatures of large scale phenomena such as meridional flows or the tachocline, and important in calibrating techniques that depend inherently on the geometry being spherical. Moreover, various systematics such as center to limb travel-time variations and fore-shortening can be investigated, given the availability of vector velocities and a $360^\circ$ view of the sphere. Indeed, while helioseismology has made great strides is peering into the solar interior, we have yet to clearly understand the ability of these methods, and most importantly, the accuracy of the inferences.

*Acknowledgements.* This work was made possible with funding from grant NASA MDI NNG05GH14G. We also thank NASA for making Columbia available to us.

## References

Berland, J., et al.: 2006, CF 35, 1459
Christensen-Dalsgaard, J., et al.: 1996, Sci 272, 1286
Duvall, T.L., Jr., et al.: 1993, Nature 362, 430.
Hanasoge, S.M., Duvall, T.L., Jr.: 2006, in: K. Fletcher (ed.), *Beyond the Spherical Sun*, ESA SP-624, p. 40.1
Hanasoge, S.M., et al: 2006, ApJ 648, 1268
Lele, S.K.: 1992, JoCoPh 103, 16
Rast, M.P., Bogdan, T.J.: 1998, ApJ 496, 527
Vichnevetsky, R., Bowles, J.B.: 1982, *Fourier Analysis Of Numerical Approximations Of Hyperbolic Equations*, SIAM, Philadelphia, pp. 72

 